Energy Equip. Sys. / Vol. 9/No. 4/Dec. 2021/ 331-349

ENERGY EQUIPSYS

Energy Equipment and Systems

http://energyequipsys.ut.ac.ir
www.energyequipsys.com

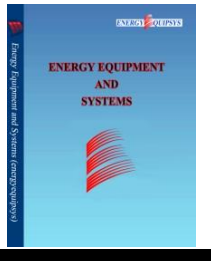

Thermo-economic analysis and optimization of a novel combination of the solar tower power plant, Stirling engine, Reverse osmosis desalination, and proton exchange membrane electrolyzer

Authors

Asadollah Arabhaghighi [a]
Mahdi Moghimi [a*]

[a] Mechanical Engineering Department, Iran University of Science and Technology, Tehran, Iran

ABSTRACT

This simulation study is aimed to investigate a multi-generation system including cycles of reverse osmosis (RO) desalination, Stirling engine, liquefied natural gas (LNG), a solar tower plant, and proton exchange membrane (PEM) electrolyzer to produce power, pure water, and hydrogen gas. All analyses were conducted to calculate the efficiency, exergy, energy, thermo-economic analysis, and total costs of this system. The sun radiation, liquefied gas flow rate, the temperature difference in the heat exchanger on the cold part of the Stirling engine are assumed as design parameters. Also, the effects of these parameters variation on hydrogen and pure water production were investigated. The power produced by the Stirling engine and LNG cycle of the proposed system is 8.18 MW (with the second law efficiency of 39.2%), which is used to produce 720 m3/h freshwater and 130.5 kg/h hydrogen gas. Sensitivity analysis was performed to determine the most effective variable on the operating conditions which indicated that solar radiation is the most effective design parameter. Finally, the total exergy efficiency and total cost rate were considered as two objective functions and the system was optimized by the Genetic algorithm. In optimized conditions, by the linear programming technique for multidimensional analysis of preference (LINMAP method), exergy efficiency becomes 43.29% and hydrogen production gets 7.6% increased.

Article history:

Received : 13 February 2021
Accepted : 18 August 2021

Keywords: Desalination, Hydrogen Production, Exergy Analysis, Economic Analysis, Genetic Algorithm.

1. Introduction

In the last century, population growth has increased the need for freshwater and energy sources. In recent decades, researchers are working on designing a feasible and novel configuration of an energy system to apply a renewable-based resource, improve efficiency, reduce greenhouse effects, and decrease the total cost[1]. While fresh water is essential to sustain human life, energy plays a significant role in the quality of life, prosperity, and economic growth of countries worldwide[2]. Water (freshwater desalination from salty sources) and hydrogen production as a clean and storable source of energy are two highly efficient sources that are vital for a growing

* Corresponding author: Mahdi Moghimi
Mechanical Engineering Department, Iran University of Science and Technology, Tehran, Iran
Email: moghimi@iust.ac.ir

population. In this regard, multi-generation systems that include several subsystems will be extensively addressed for the optimization of their entire energy content and costs.

The application of Concentrated Solar Power systems (CSP) is increasing due to their higher efficiency [3] in the case of molten salt, its mean net efficiency is about 14% which can rise to 30-40% in combination with a steam turbine cycle[4]. Chen et al. in 2018 [5] investigated key parameters for sizing the heliostat field and thermal storage in solar tower power plants. The results show that the optimal design direct normal irradiance for a minimal Levelized cost of energy depends on both the annual irradiation level and the distribution of solar irradiance.

Stirling engine is composed of two isothermal processes and one isochoric process and its efficiency are equal to the Carnot cycle under ideal conditions [6]. Hosseinpour et al. in 2017[7] analyzed a cogeneration system based on a methane-fed solid oxide fuel cell, integrated with a Stirling. They used a cooling water unit for a heat sink in a Stirling engine and that can supply the heating needs for a small home. Garrett Rinker et al. in 2018[8] studied the effect of the implementation of radiation shields in the displacer assembly of a Stirling engine. The results show that the surface finish is a critical aspect of reducing radiation losses since the higher emissivity cases resulted in higher displacer body temperatures and total heat flux to the displacer body.

Traditionally, water was used as the cold source of the Stirling engine; however, today, the LNG cycle is often used to optimize the systems[9]. Emadi et al. in 2019[10] investigated thermo-economic optimization of a new multi-generation system with a geothermal heat source and LNG heat sink. The system includes two organic Rankine, an absorption refrigeration cycle, and a PEM electrolyzer to form an efficient multi-generation system. A system design with a total cost rate of 423.5 ($/hr) and an exergy efficiency of 24.92% is obtained as the optimal solution. Akbari in 2018[11] introduced an integrated power generation and LNG recovery process. In this study, an integrated transcritical carbon dioxide Rankine cycle, Stirling power cycle, and liquefied natural gas regasification process have been analyzed. The overall energy and exergy efficiencies of the process are 37.45% and 64.26%.

Application of the reverse osmosis membrane technologies has reached 44% in the last forty years due to their enhanced quality and low costs[12]. Dimitriou et al. in 2014[13] investigated two combinations of SWRO with Clark and Danfoss pumps experimentally. Their results indicated that the specific energy consumption of the combination with the Danfoss pump is lower than a combination with the Clark pump. The second combination is suitable for future direct connections with renewable energy systems. Qureshi et al. in 2013[14] performed a sensitivity analysis on different design and performance factors of a reverse osmosis system. Their results show that the most important Design and performance parameter was the feed pressure and feed concentration. Ameri et al. in 2016[15] modeled a novel configuration of reverse osmosis, humidification-dehumidification, and flat plate collector. The results indicate that utilization of the novel configuration increases the exergy efficiency of the desalination system and the amount of freshwater production has been increased.

A combination of a proton exchange membrane electrolyzer with different sources of energy such as geothermal, wind, and solar energies has been also addressed. For instance, Nafchi et al. in 2018[16], also examined the PEME combination with a geothermal energy source. Behzadi et al. in 2018[17] studied a novel solar-based combined system which is consisting of a concentrated PV, a double effect LiBr-H2O absorption chiller, and a Proton Exchange Membrane. Furthermore, Lummen et al. in 2019[18], studied a thermo-economic analysis of waste heat recovery from condensing steam for hydrogen production by PEM electrolysis. Zhao et al. in 2018[19], investigated the transient behavior of a PEM at different step currents. Transient characteristic is one of the important indicators for evaluating dynamic performance. This article helps to better understand the dynamic response mechanism of fuel cells and evaluate their dynamic performance. Huang et al. in 2017[20], simulated a PEM system to investigate the evaporation behavior of various fuels in the evaporator coil of steam reformer used for

hydrogen gas production purposes. The simulation results indicate that pure ethanol yields the highest hydrogen production efficiency and the most suitable fuel for the steam-reforming production of hydrogen gas.

This simulation study aims to present a selective system to produce freshwater and hydrogen using renewable energy. The simultaneous application of these systems is the novelty of this paper which has not been addressed before. The solar energy as clean input energy is being transferred to the molten salt by heliostats reflectors and absorbing towers and increases the molten salt's temperature to 475 degrees; this energy is then transferred to the hot section of the Stirling engine. On the other hand, LNG serves as a heat sink for the Stirling engine due to its endothermic nature. Due to the novelty of the proposed configuration and the unknown significance of each parameter, a sensitivity analysis was conducted on the design parameters and its results can highly contribute to the selection of the optimization parameters

A	Area , effective membrane area (m^2)
$\dot{C}$	Cost rate (M$/yr)
c_p	specific heat (kJ/K)
C	Molar concentration (kmol/m^3)
Ex	Exergy flow rate (kJ/kg)
$\dot{E}$	Exergy rate (kJ/s)
F	Faraday constant (C/mol)
G	Gibbs free energy (kJ)
H	Specific enthalpy (kJ/kg)
i_{eff}	the effective annual cost of interest rate
J	Current density (A/m^2)
K	Water permeability (m^3/s. m^2.kPa)
L	Membrane thickness (μm)
LHV	Low heating value (kJ/kmol)
$\dot{m}$	Mass flow rate (kg/s)
M	Mass capacity (kg)
MW	Molar weight (kmol/kg)
$\dot{N}$	Molar mass flow rate (mol/s)
N	Number of system operating year
P	Pressure (kPa)
$\dot{Q}$	Heat (kJ/s)
R_{PEM} (Ω)	Proton exchange membrane resistance
r_r	Recovery ratio
R	Ideal gas constant. 8.314 (J/mol.K)
S	Enthalpy (kJ/K)
T	Temperature (C)
U	Internal energy (kJ/kg.s)
V	Potential (V)
$\dot{V}$	Volume flow rate (m^3/s)
$\dot{W}$	Work (kJ/s)
X	Molar friction (-)
Y	Salinity (PPM×10^6)
Z	Purchase cost ($)
$\dot{Z}$	Annual cost rate ($/yr)

Greek symbols

η	Over potential (PEM), efficiency
λ(x)	Water content at location x in the Membrane (Ω^{-1})
π	Osmosis Pressure (kPa)
ρ	Density (kg/m^3)
Σ	Local conductivity
ϕ	Maintenance factor

Subscripts and abbreviations

a	Anode
abs	Absorption
act	Activation
b	Brine
c	Cathode
Ch	Chemical
comp	Compressor
CSP	Concentrated Solar Power
des	Destruction
e	Exit
el	Element
en	Energy
ex	Exergy
exp	Expansion
f	Feed
HP	High-pressure
HS	Heliostat
HX	Heat exchanger
i	Input
irr	Irreversibility
it	Isothermal
LP	Low-pressure
MS	Molten salt
Ohm	Ohmic
P	Pump
Pr	Product

PEM Proton exchange membrane
rec Receiver
RO Reverse osmosis
s Salt
SE Stirling engine
t Turbine
tot Total
w Wate

2. System description

Figure 1 illustrates the suggested integrated multi-generation system composed of solar tower power, Stirling engine, LNG cycle, PEM electrolyzer, and RO desalination system. Molten salt is used as the operating fluid in the subsystem of solar tower power which receives the solar heat reflected by the heliostats field and transfers that to nitrogen in the heat exchanger of the hot section of the Stirling engine, in which nitrogen is expanded. Stirling engine consists of three sections; isothermal turbine, isothermal compressor, and isochoric heat exchanger. Nitrogen as the operating fluid in the isothermal turbine which is expanded by receiving heat from molten salt passes through the heat exchanger and transfers the heat to the turbine input line and enters the compressor. It is then compressed by losing its heat to the LNG cycle and produces power. The main objective of using LNG cycle is to enhance the efficiency of the Stirling engine by creating a heat sink. Besides, a cooling unit and a turbine are also located in this cycle to decrease the pressure of the operating fluid to the atmosphere and prevent energy dissipation. Finally, Stirling engine and LNG turbine will provide the required power of RO and PEM sections.

In the RO subsystem by receiving constant power, after two steps of filtration and separating coarse particles, the two-stage membrane is implemented to reach a high recovery ratio. The output salty water and the remained power enter the PEM electrolyzer where hydrogen and oxygen of the water are separated by electrical current. In the solar power tower, Phase Change Material (PCM) energy storage systems are used to increase reliability. Under stable conditions and constant temperature, the calculations assumed a complete charge of the PCM and it is being out of the circuit.

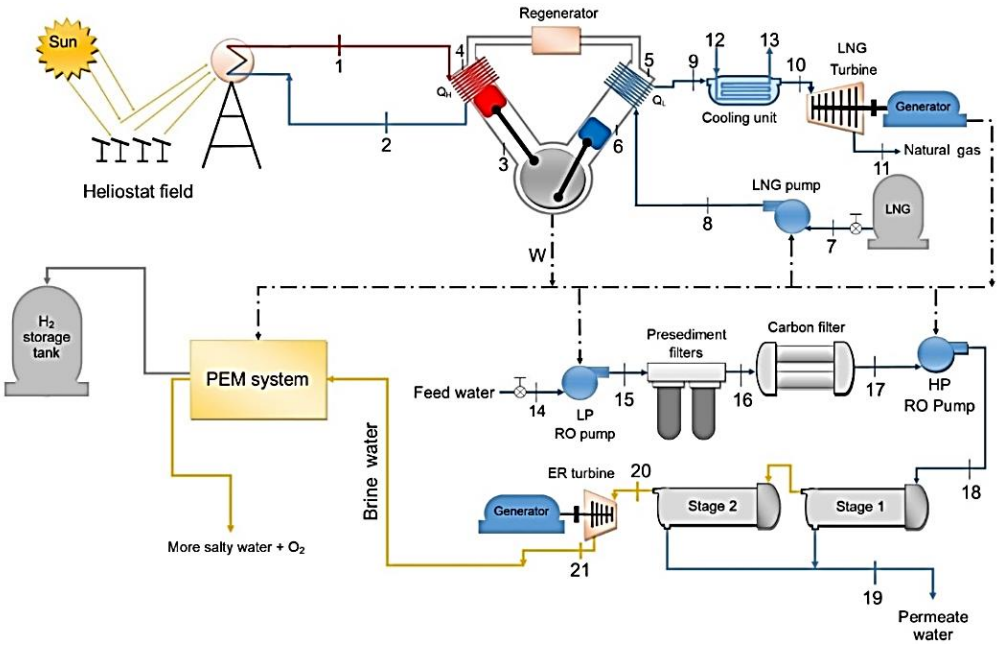

Fig. 1. Schematic of the proposed cycle

3. Mathematical modeling

3.1. Energy analysis

To design and calculate the capacity of different parts of subsystems, study their performances and the impact of some of the variables on their efficiency, a thermodynamic model is developed. To simplify the modeling, a series of assumptions were considered:

- The entire system is in a steady-state condition.
- Variations in the kinetic and potential energies were ignored.
- Pressure drop in pipes and heat exchangers were being neglected.

3.1.1. CSP tower plant subsystem

To supply the required heat for the Stirling engine, a concentrated solar power system is used. Molten salt, the working fluid of this subsystem, receives the solar heat in the central receiver and transfers it to nitrogen in the heat exchanger of the Stirling engine. Its thermophysical properties can be obtained by Eq.s (1) and (2)[21]:

$$\rho(kg/m^3)=2090-0.636\times T \quad (1)$$

$$c_P(J/kgK)=1443+0.172\times T \quad (2)$$

The heliostat field, consists of hundreds of heliostats and has a total aperture area of A, reflects and concentrates the solar radiation to the central receiver. The total isolation is proportional to the total area and can be obtained by Eq.(3)[22]:

$$\dot{Q}_{HS}=A\times\dot{q}+\dot{Q}_0 \quad (3)$$

In which $\dot{q}$ is the amount of solar radiation per unit of area. Regarding the heat dissipation and non-ideal efficiency of the different sections, the heat loss ($\dot{Q}_0$) should be considered in the heat transfer[23]:

3.1.2. LNG subsystem

According to previous studies[9], the application of the liquefied natural gas system in a Stirling engine can provide a heat sink that is more efficient in comparison with air or water cooling systems. This subsystem includes a pump, a heat exchanger with a Stirling engine, a cooling unit, and a turbine which their simplified energy conservation equations can be written as the followings:

$$\dot{W}_{LNG,\,P}=\dot{m}_{LNG}\times(h_8-h_7) \quad (4)$$

$$\dot{Q}_{LNG,\,SE}=\dot{m}_{LNG}\times(h_9-h_8) \quad (5)$$

$$\dot{Q}_{cooling\ unit}=\dot{m}_{LNG}\times(h_{10}-h_9) \quad (6)$$

$$\dot{W}_{LNG,\,T}=\dot{m}_{LNG}\times(h_{11}-h_{10}) \quad (7)$$

3.1.3. Stirling engine subsystem

Stirling engine is the main part of the multi-generation system which can provide the required power by heat and heat sink. It is assumed that Stirling engine is composed of an isothermal turbine, an isochoric heat exchanger and an isothermal compressor in which its operating fluid nitrogen goes through the isothermal compression and expansion as well as isochoric heat transfer processes and power is generated as a result of these processes. Energy conservation equations for each component and Stirling engine are summarized below [23]:

$$\dot{Q}_{comp}=T\dot{m}_{N_2}(s_6-s_5) \quad (8)$$

$$\dot{Q}_{exp}=T\dot{m}_{N_2}(s_3-s_4) \quad (9)$$

$$\dot{W}_{comp}=\dot{Q}_{comp}-\dot{m}_{N_2}(h_6-h_5)=\dot{m}_{N_2}(T(s_6-s_5)-\dot{m}_{N_2}(h_6-h_5)) \quad (10)$$

$$\dot{W}_{exp}=\dot{Q}_{exp}-\dot{m}_{N_2}(h_3-h_4)=\dot{m}_{N_2}(T(s_3-s_4)-\dot{m}_{N_2}(h_3-h_4)) \quad (11)$$

3.1.4. Reverse osmosis subsystem

Water desalination by RO method is one of this system's parts. Prior to pass of water from two major membranes, two stages of filtration are conducted on the water in order to facilitate the separation of all the suspended particles and some chemicals. This stage has a low-pressure drop which can be compensated by an initial pump (LP) in the circuit. Then water enters two membranes by a high-pressure pump, and then the separation and water desalination occurs. Equations 12-15 are used in the RO system modeling [24].

$$\pi=CRT(K) \quad (12)$$

$$\Delta P_{HP}=0.5\times(P_{18}+P_{20})-P_{19} \quad (13)$$

$$\Delta\pi=0.5\times(\pi_{18}+\pi_{20})-\pi_{19} \quad (14)$$

$$\dot{m}_{Pr}=A\times k_w\times\rho\times(\Delta P-\Delta\pi) \quad (15)$$

For exergy and economic analysis of RO system, parameters such as mean salinity, mass fraction, and molar fraction are required. In order to calculate these parameters, the related equations are listed in Table 1.

3.1.5. PEM electrolyzer

PEM electrolyzer is the second producing part of the multi-generation system which produces hydrogen by using the power output of the Stirling engine and drained water obtained from the RO subsystem. Theoretically, the required energy of PEM can be obtained by Eq.(16) in which the first term is the required electrical energy and the second section shows the required heat.

$$\Delta H=\Delta G+T\Delta S \quad (16)$$

The total amount of hydrogen output in an electrolyzer, as well as the oxygen gas and water in the outlet, can be calculated by [26]:

$$\dot{N}_{H_2,\,out}=J/2F \quad (17)$$

$$\dot{N}_{O_2,\,out}=J/4F \quad (18)$$

$$\dot{N}_{H_2O,\,out}=\dot{N}_{H_2O,\,in}-J/2F \quad (19)$$

In which J is the current density and F denoted the Faraday constant. The electrical energy and exergy of the PEM system can be calculated by the following model [26]:

$$Q_{electric}=E_{electric}=JV \quad (20)$$

$$V=V_0+\eta_{act,\,a}+\eta_{act,c}+\eta_{Ohm} \quad (21)$$

$$V_0=1.192\text{-}10^{-4}\times(T\text{-}298) \quad (22)$$

In Eq.(21), V_0 is the reversible potential calculated by the Nernst equation. $\eta_{act,\,a}$, $\eta_{act,c}$, and η_{Ohm}, are the anode-cathode, and Ohmic activation over-voltage, respectively which can be neglected in cases where the current density is not very high (J<10000 A/m^2).

Ionic resistance of the membranes is directly related to the Ohmic over-voltage with a transfer of hydrogen ions. Humidity degree, thickness, and temperature are the effective parameters on η_{Ohm}. The local conductivity can be calculated by Eq.(23) [27].

$$\sigma[\lambda(x)]=[0.5139\lambda(x)\text{-}0.326]\exp(1268(1/303\text{-}1/T)) \quad (23)$$

where x shows the membrane depth and l(x) denotes the water content which can be obtained by Eq.(24)[27]:

$$\lambda(x)=(\lambda_a\text{-}\lambda_c/L)x+\lambda_c \quad (24)$$

To calculate η_{Ohm}, Ohmic resistance should be calculated first; then Eq.(26) can be employed[28].

Table 1. Reverse osmosis additional equations [25]

Salinity	y=ppm×10^{-6}
Averaged salinity through the membrane	$\bar{y}=\frac{\dot{m}_f\times y_f+\dot{m}_b\times y_b}{\dot{m}_f+\dot{m}_b}$
Molar fraction of the salt in the feed water	$x_{s,f}=\frac{MW_w}{MW_w+MW_s\,((1/y_{s,t})\text{-}1)}$
Salt mass flow rate in the product water	$\dot{m}_{s,Pr}=y_{s,p}\dot{m}_{Pr}$
Molar fraction of the salt in the product water	$x_{s,Pr}=\frac{MW_w}{MW_w+MW_s\,((1/y_{s,pr})\text{-}1)}$
Brine mass flow rate	$\dot{m}_b=\dot{m}_t\text{-}\dot{m}_{Pr}$
Molar fraction of the salt in the brine	$x_{s,b}=\frac{MW_w}{MW_w+MW_s\,((1/y_{s,b})\text{-}1)}$
Number of the membrane element	$N_{mem}=r_r\times\dot{V}_{RO}/\dot{V}_{el}$
Area of one membrane element	$A_{mem}=\dot{m}_{el}\times y_{s,\,RO}/k_s(\bar{y}\text{-}y_{s,\,RO})$

$$R_{PEM}=\int_0^L dx/\sigma(\lambda(x)) \quad (25)$$

$$\eta_{Ohm}=JR_{PEM} \quad (26)$$

Using the Butler-Volmer equation, the over-voltage activation can be easily computed and can be rewritten for PEM electrolyzer devices as follows[27]:

$$\eta_{act,\,i}=\frac{RT}{F}\sinh^{-1}\left(J/2J_{0,\,i}\right)= \frac{RT}{F}\ln\left[\left(J/2J_{0,i}\right)+\sqrt{\left(J/2J_{0,i}\right)^2+1}\right],\quad i=a,c \quad (27)$$

To initiate the separation process, a current difference should be applied to the membranes. Equation 28 can calculate the current density by using cathode and anode activation energies[27]:

$$J_{0,\,i}=J_i^{ref}\exp\left(-E_{act,\,i}/RT\right),\quad i=a,c \quad (28)$$

To calculate the required heat for the PEM system, the heat from irreversible processes should be calculated by Eq.(29) at first:

$$Q_{irr}=2F(\eta_{act,\,a}+\eta_{act,c}+\eta_{Ohm}) \quad (29)$$

If $Q_{irr}<T\Delta S$, no external heat is required for this process; therefore, $Q_{heat,\,PEM,}$ and $E_{heat,PEM}$ are zero. If $Q_{irr}>T\Delta S$, the following values can be calculated by Eqs. (30) and (31):

$$\dot{Q}_{heat,\,PEM}=\left[T\Delta S-Q_{irr}\right]\dot{N}_{H_2O,\,reacted} \quad (30)$$

$$\dot{E}_{heat,\,PEM}=\dot{Q}_{heat,\,PEM}(1-T_0/T) \quad (31)$$

3.2. Exergy analysis

Due to irreversibility and entropy production in all the real processes as a result, calculation of exergy is one of the most important methods to determine exergy destruction. Exergy appears in four different forms: physical, chemical, kinetic, and potential exergies. Kinetic and potential exergies are negligible and can be ignored here.

Now, by writing the exergy conservation equation for all the components and their simplifications, multiple equations can be obtained which are listed in Table 2.

When energy and exergy analysis was done on the entire system, energy and exergy efficiencies were considered as the major parameters to determine the system performance. They can be used to examine the effect of any inputs parameters changes on the system performance. Exergy destruction of oxygen output is negligible in comparison with other parameters and is neglected to simplify the equations.

$$\eta_{en}=\frac{\text{Total output energy}}{\text{Total input energy}}=\frac{H_2\text{ output energy}+H_2O\text{ output energy + cooling unit output energy}}{\text{Sun input energy+ LNG input energy}} \quad (32)$$

$$\eta_{ex}=\frac{\text{Total output exergy}}{\text{Total input exergy}}=\frac{H_2\text{ output exergy}+H_2O\text{ output exergy+ cooling unit output exergy}}{\text{Sun input exergy + LNG input exergy}} \quad (33)$$

Table 2. Expressions of exergy destruction rates

#	Exergy Destruction	Formulation
1	CSP Heliostat field	$\dot{E}_d=A_{HS}\times\dot{q}_{sun}\times(1-T_0/T_{sun})-\dot{Q}_{rec,\,tot}\times(1-T_0/T_{sun})$
2	CSP Receiver	$\dot{E}_d=\dot{Q}_{rec,\,tot}\times(1-T_0/T_{rec,sur})+\dot{m}_{ms}\times(e_{f,2}-e_{f,1})$
3	LNG Turbine	$\dot{E}_d=\dot{m}_{LNG}\times(e_{f,10}-e_{f,11})-\dot{W}_t$
4	LNG Pump	$\dot{E}_d=\dot{m}_{LNG}\times(e_{f,7}-e_{f,8})-\dot{W}_P$
5	LNG cooling unit	$\dot{E}_d=\dot{m}_{LNG}\times(e_{f,9}-e_{f,10})+\dot{m}_{Cooling}\times(e_{f,12}-e_{f,13})$
6	Stirling Engine	$\dot{E}_d=\dot{Q}_{rec,abs}\times(1-T_0/T_3)+\dot{Q}_{LNG,\,SE}\times(1-T_0/T_5)-\dot{W}_{Net}$
7	RO Presediment filter	$\dot{E}_d=\dot{m}_f\times(e_{f,15}-e_{f,16})$
8	RO Carbon filters	$\dot{E}_d=\dot{m}_f\times(e_{f,16}-e_{f,17})$
9	RO Membrane	$\dot{E}_d=(\dot{m}_f\times e_{f,18})-(\dot{m}_b\times e_{f,20})-(\dot{m}_p\times e_{f,19})$
10	PEM	$\dot{E}_d=(1-\eta_{ex})\times(Q_{electric}+E_{heat,h2o}+E_{heat,\,PEM})/No.Cell$

3.3. Economic analysis

Economic analysis can be used to estimate the total cost of implementation and maintenance.

The economic analysis of a project includes investment, annual maintenance, and repair costs as well as other economy-related parameters. The first output of the economic analysis is an overall estimation of equipment costs as well as their maintenance costs according to the system capacity and performance. Total annual costs of a system can be calculated by Eqs. (34) and (35)[28]:

$$\dot{C}_{tot}=\dot{C}_{fuel}+\dot{C}_{env}+\sum_{k}\dot{Z}_{k} \quad (34)$$

$$\dot{Z}=Z\times CRF\times\phi \quad (35)$$

In Eq.(34), $\dot{C}_{fuel}$ shows the fuel cost of a system used for energy production. The studied multi-generation system uses free solar energy. Also, $\dot{C}_{env}$ denotes the costs due to greenhouse gases emissions; this system has no greenhouse emissions. Therefore, two terms of the Eq.(34) are zero. $\dot{z}_k$ is the investment and maintenance cost of equipment k. The equations related to each equipments of this studied system are presented in Table 3.

As presented in Table 3, the present year costs of the equipment costs were related to the previous years which should be modified due to inflation and other issues. To modify them, Eq.(36) and the annual cost index can be employed to the current year and previous year's costs index was obtained from the chemical engineering plant cost index, CEPCI[37].

$$\dot{Z}_{2018}=\dot{Z}\frac{CI_{2018}}{CI_{Ref\text{-}year}} \quad (36)$$

In Eq.(35), ϕ is a factor related to maintenance and repair and CRF is the cost recovery factor which can be obtained by Eq.(37). It classifies the costs and relates the annual costs for the first year. In Eq.(37), i_{eff} shows the effective gain rate and N denotes the number of expected working years as presented in Table 4.

$$CRF=i_{eff}\frac{(1+i_{eff})^{N}}{(1+i_{eff})^{N}-1} \quad (37)$$

Table 4. Economic parameters

Parameter	Value
N	20 years
i_{eff}	12 %
ϕ	1.06

Table 3. Capital cost expression of components

Component	Cost function	Ref	Cost index
	CSP tower subsystem		
Heliostats	$Z=216\times A_{HS}\times 10^{6}$	[29]	521.9
Salt-cooled receiver	$Z=3.52\times Q_{rec}^{0.44}\times 10^{6}$	[29]	521.9
Tower	$Z=(0.0305\times Q_{rec}+0961)\times 10^{6}$	[29]	521.9
	LNG subsystem		
Pump	$\dot{Z}=1120\times \dot{W}_{p}^{0.8}$	[30]	550.8
Cooling unit	$Z=2143\times A_{Cooling\ unit}^{0.514}$	[31]	576.1
Natural gas turbine	$Z=479.34\times(\dot{m}/0.93-\eta_{t})\times \ln(P_{in}/P_{out})\times (1-\exp(0.036T_{in}-54.4))$	[28]	381.7
	Reverse osmosis subsystem		
Seawater intake and pretreatment	$\dot{Z}=996\times \dot{Q}_{f}^{4/5}$	[32]	381.7
High-pressure pump	$\log_{10}\dot{Z}=3.3892+0.0536\log_{10}(\dot{W}_{HPP})+0.1538\times[\log_{10}(\dot{W}_{HP})]^{2}$	[33]	584.6
Permeator	$Z_{RO}=10N.A_{m}$	[34]	575.4
Energy recovery turbine	$\log_{10}(Z)=2.2476+1.4965\log_{10}(\dot{W}_{ERT})-0.1618[\log_{10}(\dot{W}_{ERT})]^{2}$	[33]	584.6
Stirling engine	$Z=2200\times \dot{W}_{SE}$	[35]	521.9
PEM electrolyzer	$Z=1000\times \dot{W}_{PEM}$	[36]	556.8
Hydrogen storage	$Z=500\times M_{tank}$	[37]	576.1

4. Results and discussion

4.1. Model validation

In this research, energy, exergy and economic model of the system have been developed. According to Fig.2, five models for five main parts of the multigenration system are developed separately. For validation of CSP model, the work of Xu et al. [22] was employed; their cycle was accompanied by a Rankine power cycle, For LNG and Stirling engine cycles as well as PEM, the study by Emadi et al. [25] was used and finally, the work by Sharqawy et al. [24] was employed for RO. Then the five validated models are linked together and for final check, the law of energy and Exergy has been examined on the whole system to confirm the validity of the combination. The highest error of the model was observed in the low-pressure pump of the RO system, which can be due to the elimination of the return line to regulate the TDS of the produced water. All the errors are listed in Table 5.

4.2. Model results

To investigate the condition of the system, modeling was conducted according to the algorithm shown in Fig 2.
In order to obtain the thermophysical properties of each fluid, the temperature and pressure values at the marked points in Fig. 1 are listed in Table 6.

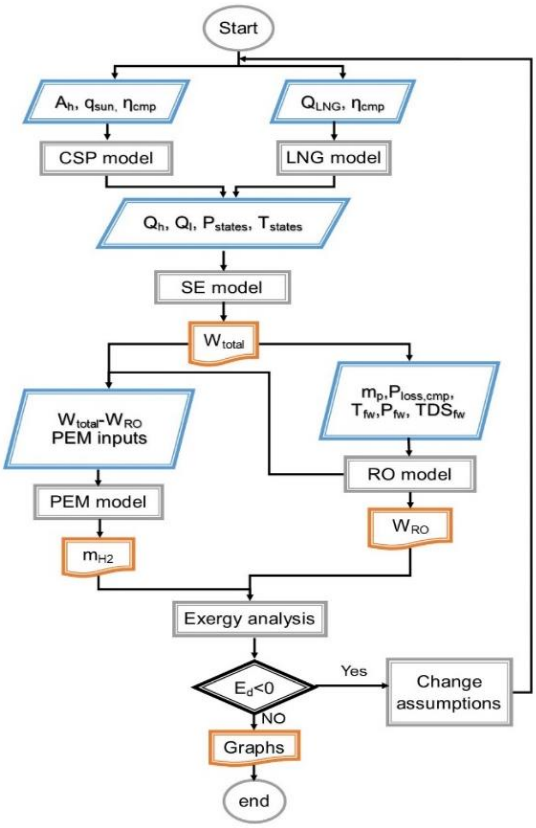

Fig. 2. The modeling block diagram.

For numerical calculations and reaching the optimal results, some of the capacities and constants were derived from the previous studies as shown in Table 7.

The values required to calculate the PEM electrolyzer power are tabulated in Table 8.

Table 5. Validation results

#	Parameters	Unit	Ref. value	Present study	Error (%)
1	Heliostat delivered energy	kW	6000	6000	0
2	Central receiver delivered energy	kW	5401.3	5400	0.024
3	Heliostat received exergy	kW	7478.8	7470.0	0.117
4	Central receiver received exergy	kW	5609,8	5602.5	0.117
5	LNG net power	MW	1.13	1.123	0.619
6	Cooler unit flow rate	kg/s	96.80	96.82	0.020
7	Nitrogen flow rate of Stirling engine	kg/s	87.1	87.13	0.034
8	RO low-pressure pump	kW	31.84	28.51	10.459
9	RO high-pressure pump	kW	133.9	134.22	0.239
10	Reverse osmosis total exergy destruction	kW	131.48	131.56	0.061
11	PEM needed power	kW	10686	10676	0.094
12	PEM exergy destruction	kW	4167.4	4166	0.034

Table 6. Pressure and temperature of the points

#	Fluid	P (kPa)	T (°C)	ṁ (kg/s)	#	Fluid	P (kPa)	T (°C)	ṁ (kg/s)
1	Molten salt	---	475	33	12	water	101	20	33
2	Molten salt	---	227.83	33	13	Water	101	5	33
3	Nitrogen	4280	351.4	27.57	14	Water	101.3	15	267
4	Nitrogen	378	351.4	27.57	15	Water	354.63	15	267
5	Nitrogen	---	-106.15	27.57	16	Water	336.19	15	267
6	Nitrogen	---	-106.15	27.57	17	Water	320	15	267
7	LNG	101	-161.41	9	18	Water	1507.9	15	267
8	LNG	6500	-158.8	9	19	Water	101.3	15	200
9	LNG	6370	-53.8	9	20	Water	1225.1	15	67
10	Natural gas	6242	10	9	21	Water	101.3	15	67
11	Natural gas	3000	-34.4	9	22	Hydrogen	101.3	15	2.17

Table 7. Simulation input data of the system [6, 16, 22]

Parameters	Unit	Value
Sun radiation, $\dot{q}_{sun}$	W/m^2	900
Heliostat area, A_{HS}	m^2	19000
Heliostat efficiency, η_{HS}	%	75
Central receiver efficiency, η_{rec}	%	90
LNG pump efficiency, η_{HS}	%	80
LNG turbine efficiency, η_{HS}	%	85
Recovery ratio of RO membrane, r_r	(-)	0.75
RO water Temp, T	°C	15
Feed water TDS	ppm	1550
Permeate water TDS	ppm	20
Permeability multiplied effective total membrane area	m^3/ s kPa	5.9×10^{-8}
Permeate flow rate per membrane element, $\dot{V}_{el}$	m^3/h	1.5
Salt permeability coefficient, k_s	m^3/m^2 s kPa	2.03×10^{-5}
water permeability coefficient, k_w	m^3/m^2 s kPa	2.05×10^{-5}

Table 8. Input data of PEM electrolyzer subsystem [38]

Parameter	Unit	Value	Parameter	Unit	Value
l_a	(-)	14	P O_2	kPa	1
l_c	(-)	10	P H_2	kPa	1
L	Mm	100	T_{PEM}	C	80
$J_{ref,a}$	A/m2	170000	T_{source}	C	100
$J_{ref,c}$	A/m2	4600	$E_{act,c}$	kJ/mol	76
LHV_{H2}	kJ/mol	242	$E_{act,a}$	kJ/mol	18

The main goal of this design was to examine the system performance under varied input conditions to produce a constant rate of hydrogen and water. For this purpose, some parameters such as the area and capacity of the heliostats field of the tower power plant and the working fluid flow of the cycles should be determined according to the production capacities. In the first stage, the production flow of the system was assumed constant, and mentioned values were determined. In the second stage, by considering constant design parameters, the system performance was examined under varying input conditions.

The total power production of the system was 8.18 MW. 94.5% of that was produced by the Stirling engine and the remaining 5.5% was produced by the LNG turbine. Other outputs are shown in Table 9.

Figure 3 shows the exergy destruction of each subsystem related to the entire system. In CSP, high exergy destruction indicates the

inability of the equipment to completely absorb the solar heat but should not be considered as a loss because that is unavoidable exergy destruction in solar systems.

Figure 4 depicts the Sankey diagram of exergy which shows the exergy of flows in the system. Total input and output exergy should be equal. According to Fig.4, the exergy of LNG fluid and sunlight were considered as inputs while the exergy destruction of the equipment and exergy of natural gas, hydrogen, and freshwater was the outputs.

Table 9. The energy analysis results

Parameter	Unit	Value
Heat received to heliostat field	MW	17.1
Heat received to the central receiver	MW	13.68
Heat input to Stirling engine	MW	12.43
Net power of LNG	kW	445.54
Net power Stirling engine	MW	7.74
Power of low-pressure RO pump	kW	67.8
Power of high-pressure RO pump	kW	967.82
Energy recovered by ERT	kW	75.82
Power of PEM subsystem	MW	7.22

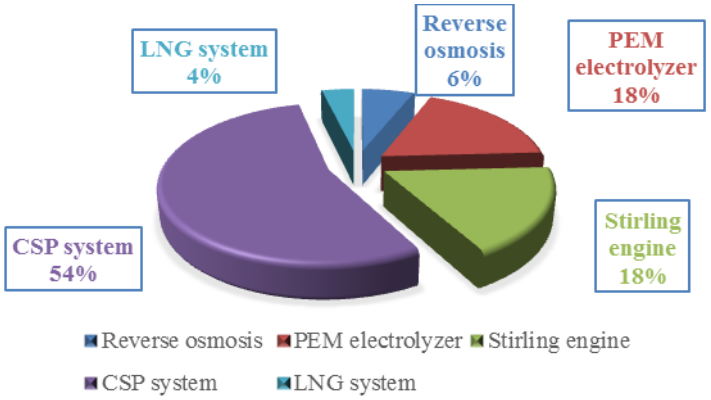

Fig. 3. Diagram of subsystems exergy destruction

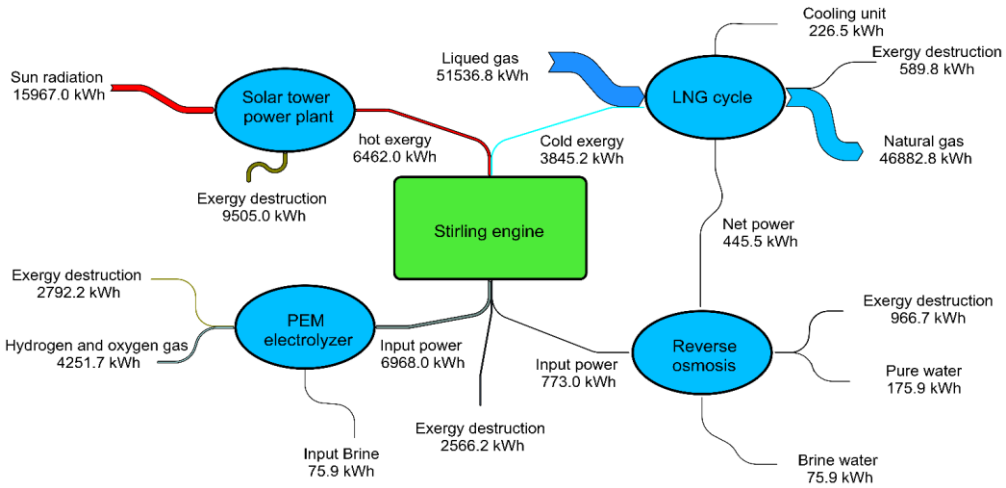

Fig. 4. Exergy flow diagram

4.3. Sensitivity analysis

Sensitivity analysis assesses the dependence of the performance parameters of a system to the changes in the design parameters. Figure 5 illustrates the sensitivity of energy efficiency, exergy efficiency and total cost rate as performance parameters. Variation of LNG flow rate from 8 to 10 kg/s, the temperature difference of LNG heat exchanger and the cold part of Stirling engine from 100 to 110° C, as well as the solar radiation from 800 to 1000 W/m^2 (winter to summer variation and solar collection efficiency affected by solar angle), were considered as three design parameters. According to the diagram, exergy efficiency and cost rate showed the highest sensitivity to the variation of solar radiation. Therefore, for having better design and maximum performance, the amount and range of changes in the system's operating location should be carefully measured and specified.

4.4. Parametric study

In this section, the impact of design parameters variations due to weather changes and equipment will be investigated. These important design parameters are the same as the sensitivity analysis section. While the influence of variation of each parameter on the system performance is studied, the rest of the parameters are kept constant. Variation of exergy destruction of systems, total energy and exergy efficiency, total cost rate, and amount of hydrogen production as performance parameters of the system will be illustrated in this section.

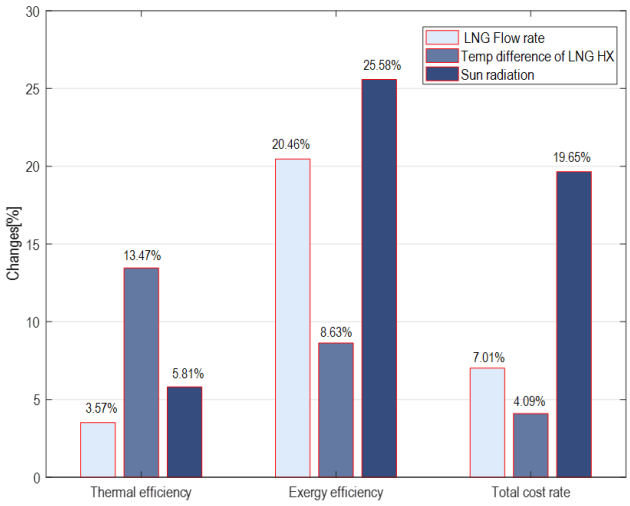

Fig. 5. Sensitivity analysis diagram

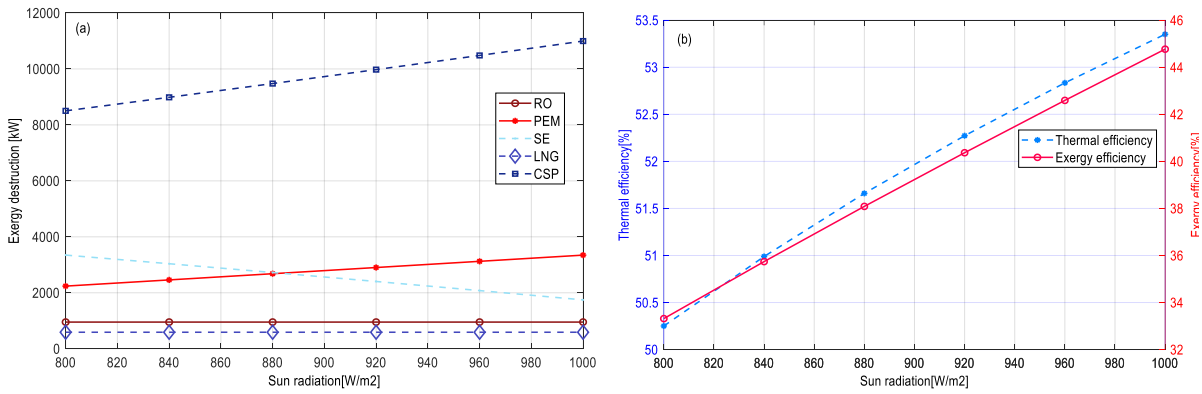

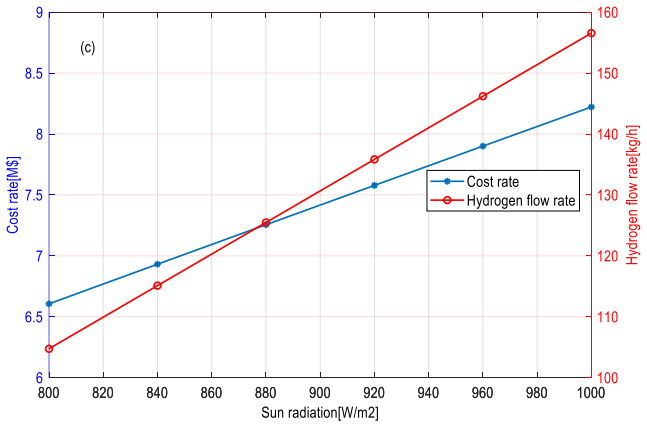

Fig. 6. Exergy destruction (a), efficiencies (b), and production and cost rate (c) changes with sun radiation

The sun radiation is equal to the input hot exergy and is one of the parameters which change daily by environmental conditions. Figure 6 (a) illustrates the exergy destruction of the five subsystems concerning sun radiation. CSP subsystem exhibited the highest exergy destruction which shows how much of the accessible sun radiation could be gained. In the Stirling engine, the variation of this parameter changed the heat received by the CSP subsystem which resulted in higher power production according to the first law of thermodynamics. Considering the Stirling engine as a control volume and investigating the amount of exergy destruction, it was observed that with the increase of the input heat, the input exergy flow increased by a coefficient below one; while the increase of output exergy flow was with coefficient one. Overall, its exergy destruction decreased by the increase of solar radiation. One of the initial assumptions of the multi-generation system modeling was the constant RO production flow rate which allocated a constant amount of power to itself. Therefore, changing the other parameters does not affect this subsystem. However, change in the total power production can vary the receiving power of PEM and hence vary the hydrogen production flow rate and finally its exergy destruction.

Figure 6 (b) illustrates the total energy and exergy efficiencies of the system. As shown in Fig. 6 (a), total exergy destruction increased by sun radiation enhancement; therefore, the total efficiency should be decreased. However, the system exergy and energy efficiencies depend on the production rate. Regarding hydrogen production enhancement, the overall efficiency of the system increased. Figure 6 (c) also represents the total cost of the system and the main output flow rate of the system e.g. the hydrogen production. The increase of sun radiation increased the accessible power and hence enhanced hydrogen production.

During system design, complete study and accurate measurement of the environment are of critical importance. The sun radiation should be measured with high accuracy, if its precise value was not available and the system assumed its high abundance, the system would have high capacity and cost due to the direct dependence of the components cost to the consumed power. However, as the required amount of solar radiation was not accessible, the assumed production and efficiency will be impossible as can be seen in Fig 6 (c).

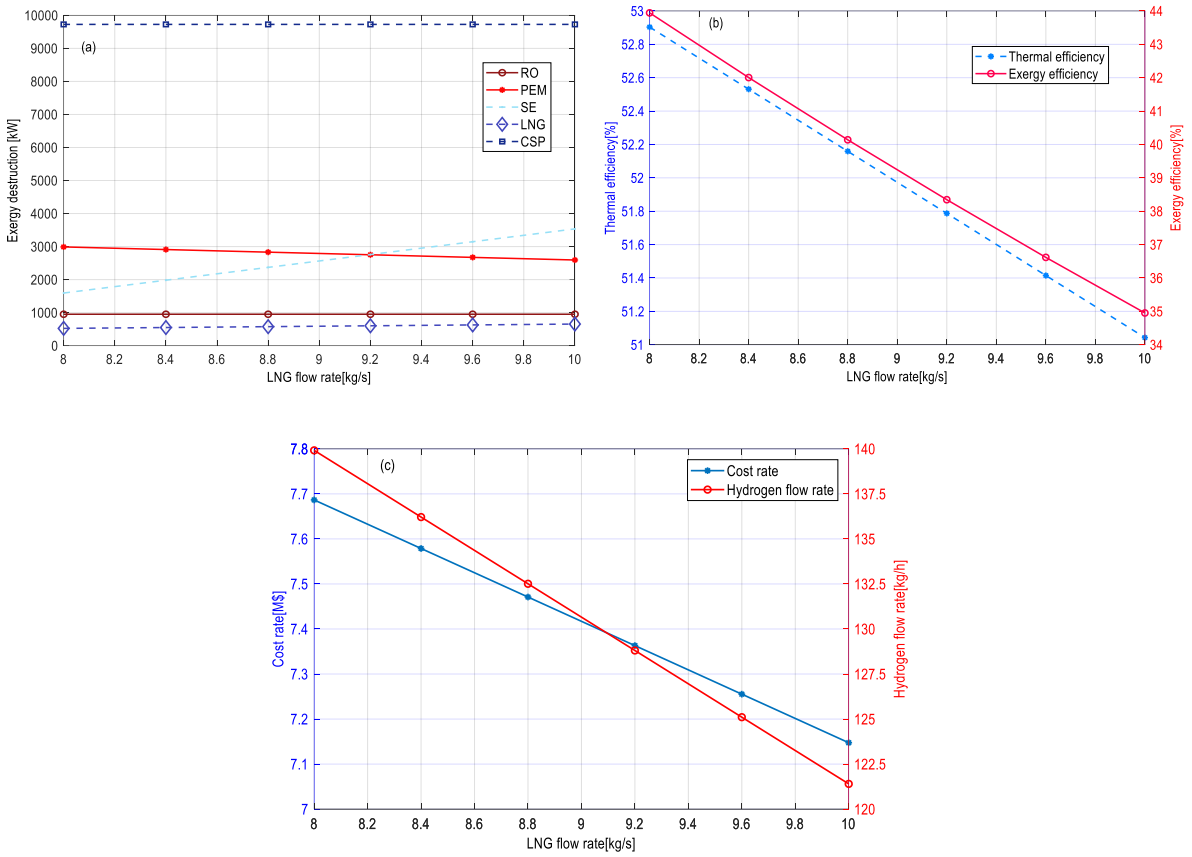

Fig. 7. Exergy destruction (a), efficiencies (b), and production and cost rate (c) changes with the LNG flow rate

The LNG flow rate as input cold exergy was among the parameters in which its values should be investigated carefully, the impact of this parameter on exergy destruction for each subsystem is illustrated in Fig 7 (a). By variation of this parameter from 8 to 10 kg/s, the total exergy destruction of the LNG subsystem will increase from 25%. With increasing the flow rate, the losses also rise, hence the exergy destruction will be increased. By increasing this parameter, the amount of the applied cold load to the Stirling engine will also increase which according to the first law of thermodynamics will reduce the produced power and increase the exergy destruction. According to diagram (a), the exergy destruction of PEM system was decreased. As shown in Fig 7 (c), hydrogen production was also declined which could be due to decreased power production of the system.

With the increase of the LNG flow rate, more exergy will be entered into the system which leads to expecting an increase in hydrogen production and enhancement of total efficiency. However, in reality, this can increase the Stirling engine exergy destruction by keeping the hot exergy constant, and decreasing the hydrogen production, so, the energy and exergy efficiencies will be declined as shown in Fig 7 (b).

According to what was stated above, an increase in the LNG flow rate decreased the available power and as a result, the hydrogen production will be decreased as shown in Fig7 (c). By increasing the LNG flow rate, the costs will be declined as a result of power decreasing. In this case, for systems designed for high capacities, it will result in not being able to exploit the total implementation cost.

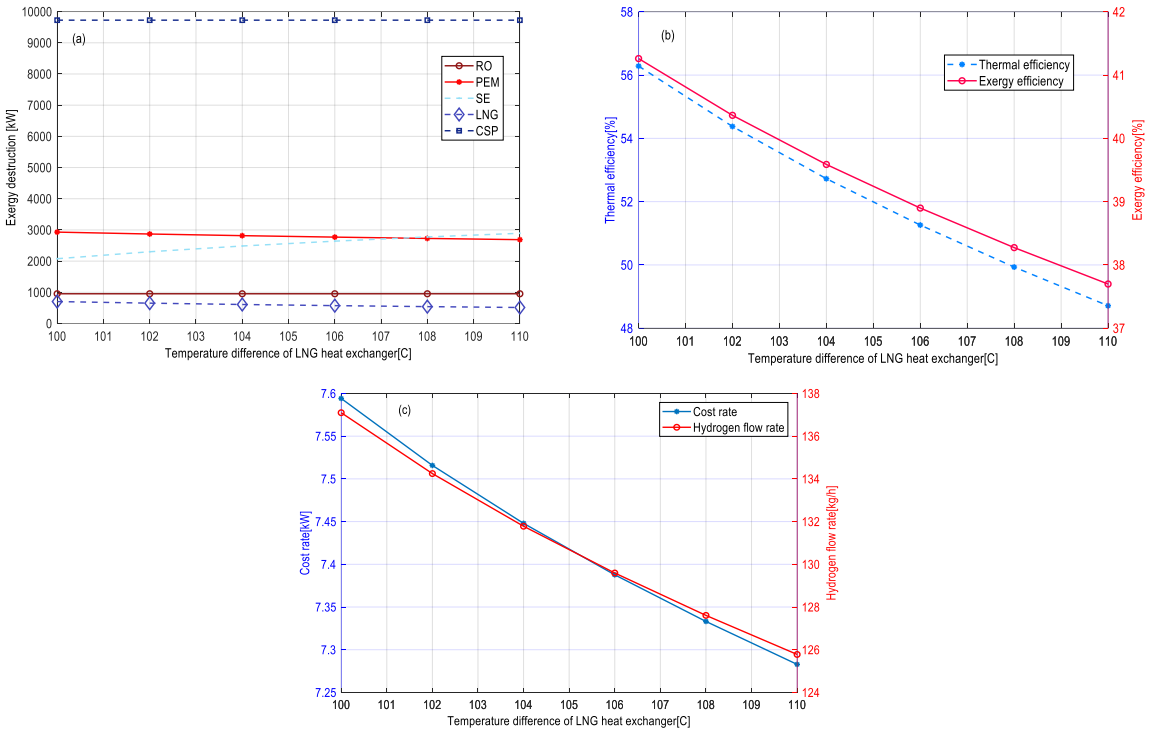

Fig. 8. Exergy destruction (a), efficiencies (b), and production and cost rate (c) changes with a temperature difference of LNG heat exchanger

An increase in temperature difference between the inlet and outlet for fluid in the heat exchanger indicates more efficient heat transfer which can decrease the exergy destruction. According to Fig 8 (a), the exergy destruction of the LNG system decreased due to the lowering of its heat exchanger exergy destruction. The amount of heat absorbed from the Stirling engine is also enhanced by the increase of heat exchanger efficiency. From the other side, Constant heat input will decline the expansion and decline the power production by the Stirling engine and hence the power accessible for PEM. Therefore, the exergy destruction of Stirling is increased while it decreases in the PEM system.

In Fig 8 (b), the total efficiency and production of the system are shown. As stated before, with the increase of the cold energy in the Stirling engine and constant hot energy, the power production will be declined, and this will decrease the system efficiency. The exergy destruction increased and hence the total exergy efficiency was declined. Hydrogen production of the system, as well as exploitation cost, will be declined as shown in Fig 8 (c).

5. Optimization

In the optimization section, the optimal values of the objective functions will be determined by the simultaneous change of the parameters in the definite range. Total cost and total exergy were two studied objective functions that were optimized by a Genetic algorithm. Table 10 shows the optimization parameters and their variation range. Optimizing sun radiation is only done for selecting a better place for installation total system if there were some options.

Table 10. The range of design parameter variation

Variable	Unit	Range
Sun radiation	W/m^2	800-1000
LNG flow rate	kg/s	8-10
Temp difference of LNG heat exchanger	˚C	100-110

There is no particular algorithm to achieve the best solution for all optimization problems. Also, most algorithms cannot simultaneously provide accuracy and velocity of proper convergence for all optimization problems[39]. Emperor Penguins Colony, Momentum Balance Algorithm (MBA) algorithms, Water cycle

algorithm, and metaheuristic bat-inspired algorithm are some new optimization methods. In most optimization methods, having a high number of repetitions leads to an accurate answer and the difference between these methods is in the running time. Genetic algorithm due to having some advantages like Parallelism, Inherently parallel, Large and wide solution space searchability and etc. In this study, GA method was selected for optimization due to the required characteristics and low-resolution time

Simultaneous optimization of two objective functions was conducted by multi-objective optimization in MATLAB. In the first stage of the genetic algorithm, a group of solutions was formed by inputs. By multiplication and growth of the solutions, the optimal condition will be approached. Finally, LINMAP and TOPSIS methods were employed to select a solution as the optimal one for both objective functions. Before these, the obtained solutions needed to become dimensionless which was conducted by the Euclidian method as mentioned in Eq. (38)[39].

$$F_{ij}^{n} = \frac{F_{ij}}{\sqrt[2]{\sum_{i=1}^{m}(F_{ij})^{2}}} \qquad (38)$$

Figure 10 shows the Pareto front of the optimization, which was plotted after obtaining the dimensionless values by the Euclidian method. Points A and B were considered as the optimal solutions for the first and second objective functions, respectively. LINMAP and TOPSIS, which were plotted, based on the distance between the ideal and non-ideal points are the optimal conditions for both objective functions.

The optimized variable of each point of Fig. 9 is shown in Table 11.

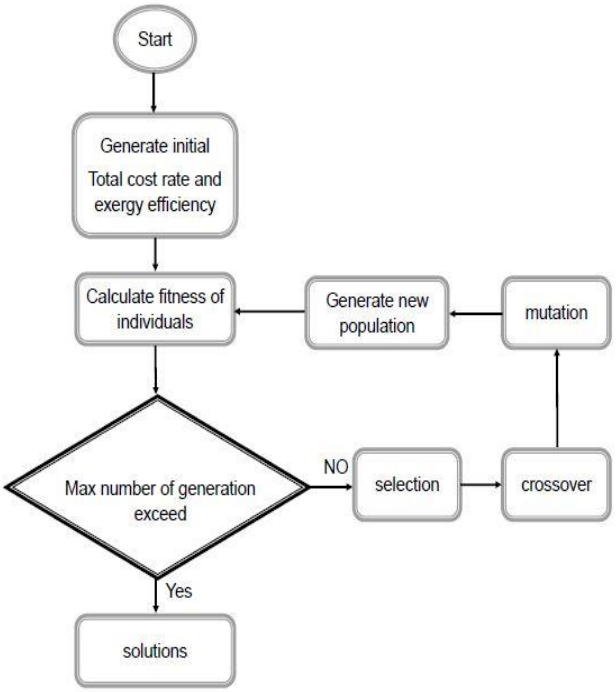

Fig. 9. The genetic algorithm scheme.

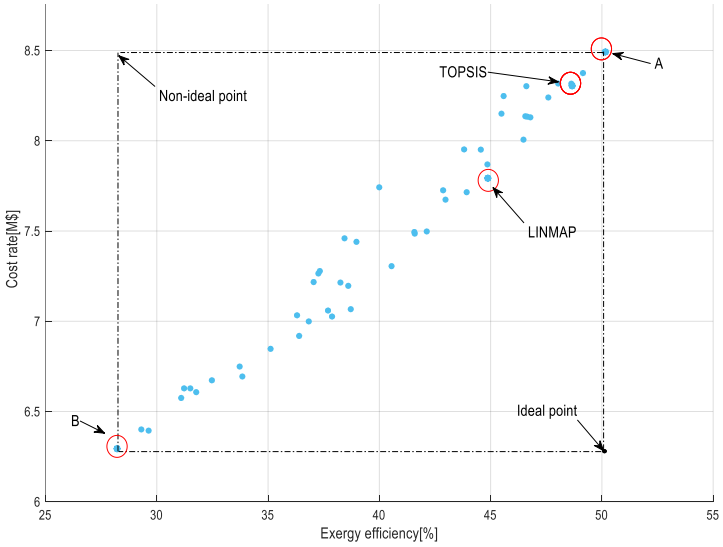

Fig. 10. The Pareto frontier for optimization results

Table 11. The optimized value of design parameters

Point	Objective function value		Design parameters optimized value		
	η_{ex}(%)	$\dot{C}_{tot}$(M$/yr)	$q_{sun}(W/m^2)$	$\dot{m}_{LNG}$(kg/s)	$\Delta T_{HX,LNG}$
First selected point	39.2	7.4	900	9	105
A(1st obj maximizing)	52.00	8.59	990.74	8.01	100.44
B(2nd obj minimizing)	29.39	6.30	809.4	10.00	110
LINMAP	43.29	7.74	908.4	8.34	103.47
TOPSIS	48.82	8.37	967.63	8.08	100.88

Having the highest exergy efficiency of the system along with the most cost-effective is the main goal of optimization. In order to achieve those values, the input parameters that can be changed in a certain interval must be changed during the design to determine their optimal value. According to the values of Table 11. The mode selected by the LINMAP method will be optimized with the least change in input parameters. In the TOPSIS method, compared to the LINMAP, by increasing the cost rate by 8%, a 12% higher exergy efficiency can be achieved than in the LINMAP mode.

6. Conclusion

A multi-generation system was investigated to produce fresh water and hydrogen gas by sun radiation. Energy, exergy, thermo-economic and sensitivity analysis, as well as optimization of the variables, were performed. Stirling engine and LNG turbine cycle are the two major parts of the power production in the system. By using the accessible power, 720 m^3/h freshwater and 138 kg/s hydrogens can be produced. According to the exergy analysis of the system and input and output flows, CSP solar tower power had the highest exergy destruction which indicates incomplete use of the radiated sun radiation. According to sensitivity analysis on the system performance, it was revealed that the mean daily solar radiation should be closely addressed during designing the project and locating its site so that the highest performance can be achieved. LNG flow rate, the temperature difference of LNG heat exchanger of cold part of Stirling engine and the sun radiation were the design parameters and a multi-objective optimization was conducted based on genetic algorithm. After obtaining a series of points, the optimal ones of the two objective functions, total exergy efficiency, and total cost were determined using LINMAP and TOPSIS methods. In LINMAP optimum point, exergy efficiency gets 10.4% increased and in TOPSIS optimum point, exergy efficiency gets 24.5% increased compared to the first point, but the total cost rate of the second point is 8.1% more than the first point.

7. Declaration

7.1. Funding

In terms of science, the corresponding author supports the accuracy of equations and coding done in this article.

7.2. Conflicts of interest

On behalf of all authors, the corresponding author states that there is no conflict of interest.

7.3. Availability of data and material

All data and information about subsystems are available in the main articles to which they are referred.

7.4. Code availability

The code of the system are developed in MATLAB and optimization is performed with multivariate GA optimization tool.

References

[1] I. Fakhari, A. Behzadi, E. Gholamian, P. Ahmadi, A. Arabkoohsar, Design and tri-objective optimization of a hybrid efficient energy system for tri-generation, based on PEM fuel cell and MED using syngas as a fuel, Journal of Cleaner Production, 290 (2021) 125205.

[2] M. Vojdani, I. Fakhari, P. Ahmadi, A novel triple pressure HRSG integrated with MED/SOFC/GT for cogeneration of electricity and freshwater: Techno-economic-environmental assessment, and multi-objective optimization, Energy

Conversion and Management, 233 (2021) 113876.
[3] S. Guillot, A. Faik, A. Rakhmatullin, J. Lambert, E. Veron, P. Echegut, C. Bessada, N. Calvet, X. Py, Corrosion effects between molten salts and thermal storage material for concentrated solar power plants, Applied Energy, 94 (2012) 174-181.
[4] H. Müller-Steinhagen, F. Trieb, Concentrating solar power, A review of the technology. Ingenia Inform QR Acad Eng, 18 (2004) 43-50.
[5] R. Chen, Z. Rao, S. Liao, Determination of key parameters for sizing the heliostat field and thermal energy storage in solar tower power plants, Energy Conversion and Management, 177 (2018) 385-394.
[6] M. Moghimi, M. Khosravian, Exergy optimization for a novel combination of organic Rankine cycles, Stirling cycle and direct expander turbines, Heat and Mass Transfer, 54 (2018) 1827-1839.
[7] J. Hosseinpour, M. Sadeghi, A. Chitsaz, F. Ranjbar, M.A. Rosen, Exergy assessment and optimization of a cogeneration system based on a solid oxide fuel cell integrated with a Stirling engine, Energy Conversion and Management, 143 (2017) 448-458.
[8] G. Rinker, L. Solomon, S. Qiu, Optimal placement of radiation shields in the displacer of a Stirling engine, Applied Thermal Engineering, 144 (2018) 65-70.
[9] M.A. Emadi, H. Pourrahmani, M. Moghimi, Performance evaluation of an integrated hydrogen production system with LNG cold energy utilization, international journal of hydrogen energy, 43 (2018) 22075-22087.
[10] M.A. Emadi, J. Mahmoudimehr, Modeling and thermo-economic optimization of a new multi-generation system with geothermal heat source and LNG heat sink, Energy Conversion and Management, 189 (2019) 153-166.
[11] N. Akbari, Introducing and 3E (energy, exergy, economic) analysis of an integrated transcritical CO2 Rankine cycle, Stirling power cycle and LNG regasification process, Applied Thermal Engineering, 140 (2018) 442-454.
[12] M.W. Saleem, Y.A.C. Jande, W.S. Kim, Pure water and energy production through an integrated electrochemical process, Journal of Applied Electrochemistry, 47 (2017) 315-325.
[13] E. Dimitriou, E.S. Mohamed, C. Karavas, G. Papadakis, Experimental comparison of the performance of two reverse osmosis desalination units equipped with different energy recovery devices, Desalination and Water Treatment, 55 (2015) 3019-3026.
[14] B.A. Qureshi, S.M. Zubair, A.K. Sheikh, A. Bhujle, S. Dubowsky, Design and performance evaluation of reverse osmosis desalination systems: An emphasis on fouling modeling, Applied Thermal Engineering, 60 (2013) 208-217.
[15] M. Ameri, M.S. Eshaghi, A novel configuration of reverse osmosis, humidification-dehumidification and flat plate collector: Modeling and exergy analysis, Applied Thermal Engineering, 103 (2016) 855-873.
[16] F. Moradi Nafchi, E. Baniasadi, E. Afshari, N. Javani, Performance assessment of a solar hydrogen and electricity production plant using high temperature PEM electrolyzer and energy storage, International Journal of Hydrogen Energy, 43 (2018) 5820-5831.
[17] A. Behzadi, E. Gholamian, E. Houshfar, M. Ashjaee, A. Habibollahzade, Thermoeconomic analysis of a hybrid PVT solar system integrated with double effect absorption chiller for cooling/hydrogen production, Energy Equipment and Systems, 6 (2018) 413-427.
[18] N. Lümmen, A. Karouach, S. Tveitan, Thermo-economic study of waste heat recovery from condensing steam for hydrogen production by PEM electrolysis, Energy Conversion and Management, 185 (2019) 21-34.
[19] J. Zhao, Q. Jian, L. Luo, B. Huang, S. Cao, Z. Huang, Dynamic behavior study on voltage and temperature of proton exchange membrane fuel cells, Applied Thermal Engineering, 145 (2018) 343-351.
[20] P.H. Huang, J.K. Kuo, S.J. Tsai, Y.C. Tsai, Evaporation analysis of different fuels in evaporator coil of steam reformer for stationary PEM fuel cell systems, Applied Thermal Engineering, 128 (2018) 564-577.
[21] A.B. Zavoico, Solar Power Tower Design Basis Document, Revision 0; TOPICAL, 2001.

[22] C. Xu, Z. Wang, X. Li, F. Sun, Energy and exergy analysis of solar power tower plants, Applied Thermal Engineering, 31 (2011) 3904-3913.
[23] H. Dong, L. Zhao, S. Zhang, A. Wang, J. Cai, Using cryogenic exergy of liquefied natural gas for electricity production with the Stirling cycle, Energy, 63 (2013) 10-18.
[24] M.H. Sharqawy, S.M. Zubair, J.H. Lienhard, Second law analysis of reverse osmosis desalination plants: An alternative design using pressure retarded osmosis, Energy, 36 (2011) 6617-6626.
[25] R.S. El-Emam, I. Dincer, Thermodynamic and thermoeconomic analyses of seawater reverse osmosis desalination plant with energy recovery, Energy, 64 (2014) 154-163.
[26] H. Nami, E. Akrami, F. Ranjbar, Hydrogen production using the waste heat of Benchmark pressurized Molten carbonate fuel cell system via combination of organic Rankine cycle and proton exchange membrane (PEM) electrolysis, Applied Thermal Engineering, 114 (2017) 631-638.
[27] V. Gurau, F. Barbir, H. Liu, An Analytical Solution of a Half-Cell Model for PEM Fuel Cells, Journal of The Electrochemical Society, 147 (2000) 2468-2468.
[28] A. Bejan, G. Tsatsaronis, M.J. Moran, Thermal design and optimization, Wiley1996.
[29] G.J. Nathan, D.L. Battye, P.J. Ashman, Economic evaluation of a novel fuel-saver hybrid combining a solar receiver with a combustor for a solar power tower, Applied Energy, 113 (2014) 1235-1243.
[30] D.F. Cheddie, R. Murray, Thermo-economic modeling of a solid oxide fuel cell/gas turbine power plant with semi-direct coupling and anode recycling, International Journal of Hydrogen Energy, 35 (2010) 11208-11215.
[31] G. Xu, F. Liang, Y. Yang, Y. Hu, K. Zhang, W. Liu, An improved CO2 separation and purification system based on cryogenic separation and distillation theory, Energies, 7 (2014) 3484-3502.
[32] N.M. Wade, Technical and economic evaluation of distillation and reverse osmosis desalination processes, Desalination, 93 (1993) 343-363.
[33] R.C.B.W.B.W.J.A.S. R Turton, Analysis,synthesis and design ofchemical processes , 4th ed, pearson Education, (2012).
[34] A.M. Helal, S.A. Al-Malek, E.S. Al-Katheeri, Economic feasibility of alternative designs of a PV-RO desalination unit for remote areas in the United Arab Emirates, Desalination, 221 (2008) 1-16.
[35] D. Sánchez, R. Chacartegui, M. Torres, T. Sánchez, Stirling based fuel cell hybrid systems: An alternative for molten carbonate fuel cells, Journal of Power Sources, 192 (2009) 84-93.
[36] V. Zare, A comparative exergoeconomic analysis of different ORC configurations for binary geothermal power plants, Energy Conversion and Management, 105 (2015) 127-138.
[37] Chemical Engineering - Chemical Engineering essentials for the global chemical processing industries (CPI).
[38] E. Akrami, A. Chitsaz, H. Nami, S.M.S. Mahmoudi, Energetic and exergoeconomic assessment of a multi-generation energy system based on indirect use of geothermal energy, Energy, 124 (2017) 625-639.
[39] H. Sayyaadi, R. Mehrabipour, Efficiency enhancement of a gas turbine cycle using an optimized tubular recuperative heat exchanger, Energy, 38 (2012) 362-375.